Quart. J. R. Met. Soc. (1977), **103**, pp. 499–510

551.515.31

On the choice of radial boundary conditions for numerical models of sub-synoptic vortex flows in the atmosphere, with application to dust devils

By L. M. LESLIE and R. K. SMITH

Australian Numerical Meteorology Research Centre, P.O. Box 5089AA, Melbourne, Australia, 3001

Department of Mathematics, Monash University, Clayton, Australia, 3168

(Received 9 November 1976)

SUMMARY

This paper is a sequel to the recent numerical study of thermally driven vortices by the authors. The model developed earlier is used as a basis for comparing a variety of radial boundary conditions and to assess their suitability for models of 'tall–thin' atmospheric vortices, in particular dust devils. We have also determined those aspects of vortex dynamics which are least sensitive to the choice of radial boundary condition, and those which have a stronger dependence. The results confirm the suitability of the boundary conditions used in the earlier study, for the purposes for which that study was intended, but more realistic boundary conditions are obtained for a dust devil model.

The discussion should provide useful guidance in the design of future observational studies of dust devils and their immediate environment, and in the formulation of models for other types of sub-synoptic-scale vortices such as tornadoes and waterspouts.

1. INTRODUCTION

Observational data are not yet sufficient to enable the sources of environmental vorticity for concentrated atmospheric vortices on the sub-synoptic scale (e.g. tornadoes, waterspouts and dust devils) to be determined with surety, although they have in each case enabled the most likely ones to be identified. This uncertainty has been reflected in the interpretation of laboratory and numerical simulations of concentrated vortices which purport to model atmospheric counterparts, and it is often difficult to judge which features of a particular model are special to that model alone (perhaps due to the way in which the rotational motion is imposed, or to the way in which the vortex is constrained by boundaries), and which features are typical of a range of vortex flows and not wholly or largely due to a particular characteristic of the model.

In this paper we shall examine these questions as they relate to the problem of formulating a realistic model for a dust devil, but much of our discussion is pertinent also in modelling tornadoes and waterspouts. The work is an extension of our recent investigation of buoyant vortices (1976, hereafter referred to as I), in which a numerical model was developed to study the dynamics and structure of a vortex core driven thermally from below, with the particular aim of unravelling the close interplay between the force fields due to rotation, pressure gradient, and buoyancy. Although not realistic in certain aspects, the model contains the essential ingredients which are believed to lead to dust devils, i.e. strong thermal heating from below in the presence of rotation, and our findings appear to provide a useful basis for understanding observations of dust devil structure. We now go on to consider what changes to the model would bring it closer to one for a dust devil. Our main emphasis will be on the choice of the outer radial boundary condition, which is especially crucial to a satisfactory representation of the dust devil environment.

2. THE MODEL: PROTOTYPE AND VARIANTS

The numerical model described in I combines features of the laboratory vortex flows studied by Barcilon (1967) and Fitzgarrald (1973) and corresponds broadly with an experi-

mentally realizable situation. The region of flow for which computations are performed is cylindrical with radius R and height H and has its axis vertical. It is bounded by a rigid (no slip) lower boundary and is constrained at the side by a thermally insulated, rigid, impermeable upper portion together with a rotating, porous, lower portion with fixed height h, through which fluid with ambient temperature T_e may enter the cylinder, acquiring rotation as it does so. The flow is assumed to be axisymmetric and is driven by maintaining a circular portion of the lower boundary, with radius R_s, at a fixed temperature T_s, higher than T_e. Fluid is allowed to enter or leave the region normally through the upper boundary at which level it is assumed that vertical heat transfer is by advection only.

The fluid has density ρ and temperature T and the diffusivities of momentum and heat, K_M and K_H, are taken to be constant, and in this paper to be equal. The equations and notation are as given in I; suffice it to say that velocity components (u, v, w) are referred to a cylindrical coordinate system (r, θ, z), coaxial with the flow domain. With this notation, the boundary conditions conforming with the description given above are displayed in Fig. 1(a). The equations of motion are integrated from an initial state of no motion and uniform temperature T_e until a steady vortex is obtained and in this paper, as in I, only steady-state situations are discussed.

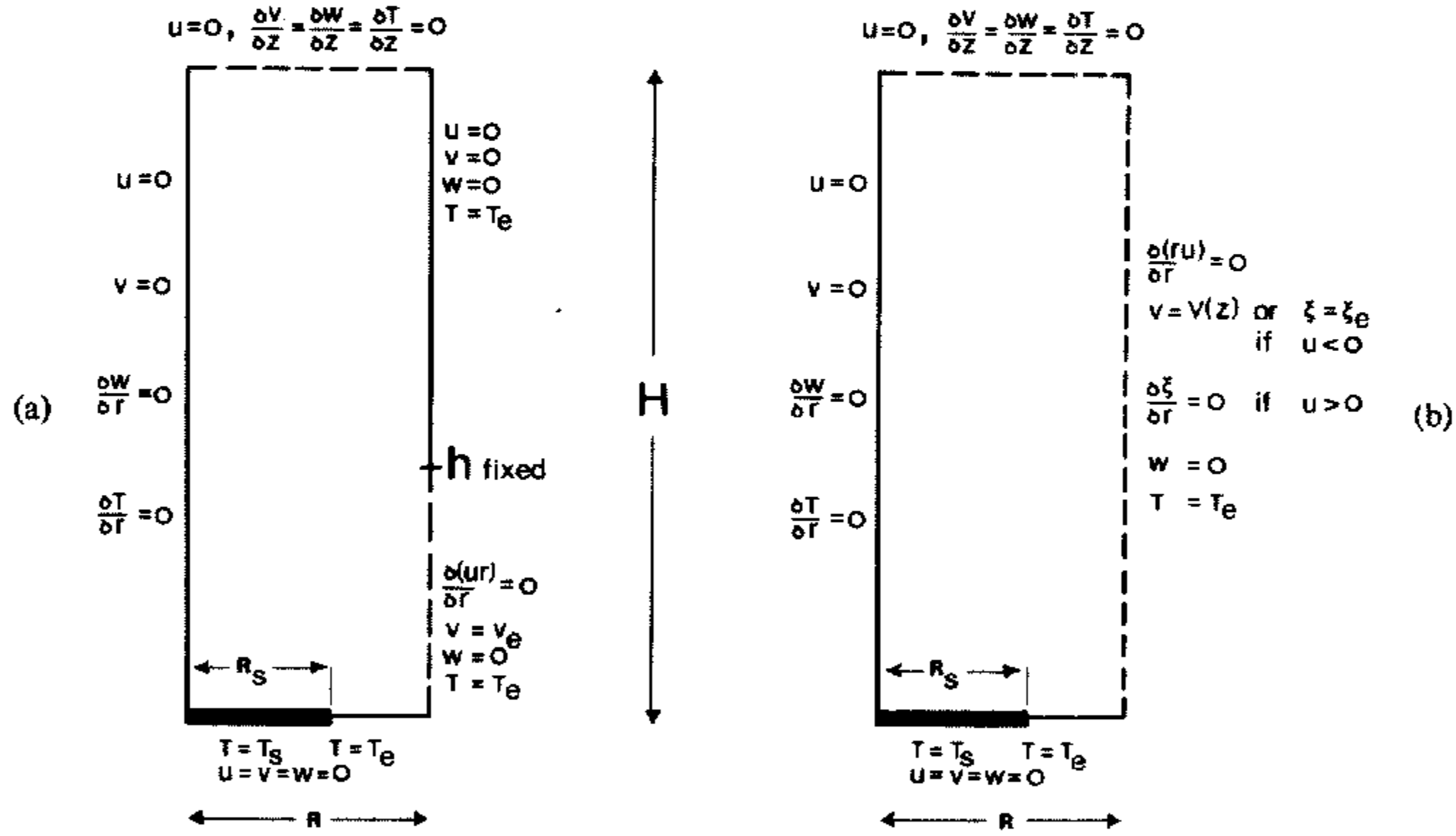

Figure 1. Boundary conditions for the numerical experiments. (a) is for Expt. 1 which is regarded as the prototype calculation and is identical to Expt. 2 of I. (b) is for Expts. 2 to 10. In Expts. 2 to 7, $v(R, z) = V(z)$ is prescribed for $0 < z < h$; in Expts. 2, 4, 5, 6 $V(z) = V_e$; in Expt. 3, $V(z) = V_e\{1 - \exp(-z/z_0)\}$ with $z_0/H = 0{\cdot}1$; in Expt. 7, $V(z) = V_e\{1 + (z/z_0)^4\}^{-\frac{1}{4}}$ with $z_0/H = 0{\cdot}1$; in each case V_e being a constant. In Expts. 8, 9 and 10, the condition on $v(R, z)$ for $0 < z < h$ is replaced with $\zeta(R, z) = \zeta_e$, a constant. In Expts. 5, 9 and 10, free slip ($\partial u/\partial z = 0$, $\partial v/\partial z = 0$) instead of no slip is imposed on the outer portion of $z = 0$: see text.

The flow depends on two main dimensionless parameters: a pseudo-Rayleigh number, $Ra = g(T_s - T_e)R_s^3/T_eK_M^2$, which characterizes the strength of buoyancy forces compared with viscous forces, and a swirl parameter, $Rt = (V_e/V_T)(R/R_s)$, which is a measure of the rotational constraint for a given level of thermal forcing and a given source radius; V_e being the tangential velocity of the screen, and V_T a thermal velocity scale defined by $V_T = \{g(T_s - T_e)R_s/T_e\}^{\frac{1}{2}}$. The factor R/R_s is included in the definition of Rt so that the latter is unchanged if R is changed while keeping the circulation imposed at that radius constant (see section 3). The other parameters have the form of aspect ratios: $A_1 = h/H$, $A_2 = R/H$, $A_3 = R_s/R$.

For reasons discussed in I, concentrated vortices will result only for a certain range of values of Ra and Rt, and we chose there values for $T_e, T_s, R_s, R, H, V_e, K_M$ typical of the laboratory experiments of Barcilon and Fitzgarrald, recognizing that there is inevitably a source of uncertainty in the value ascribed to K_M.

Our aim in the present work is to model a dust devil more closely and we must seek a more appropriate boundary condition at $r = R$. We must also use a more suitable set of values for $T_e, \ldots, K_M$, but in doing this, we should like to use the same nondimensional parameter values as in I to facilitate comparison of the present calculations with the earlier ones. Fortunately, there appears to be a close dynamic similarity between the experimental vortices and dust devils and by choosing the same dimensionless parameters as in Expt. 2 of I, we can obtain values for $T_e, \ldots, K_M$ which are broadly representative of a dust devil. Thus, with $Ra = 1{\cdot}5 \times 10^5$, $Rt = 0{\cdot}08$, $R_s/R = 0{\cdot}5$, $R/H = 0{\cdot}3$, we choose $R_s = 20\,\mathrm{m}$, $R = 40\,\mathrm{m}$, $H = 133\,\mathrm{m}$, $T_s = 350\,\mathrm{K}$, $T_e = 300\,\mathrm{K}$, and obtain $V_e = 0{\cdot}23\,\mathrm{m\,s^{-1}}$, $V_e/R = 5{\cdot}8 \times 10^{-3}\mathrm{s^{-1}}$, $K_M = 0{\cdot}6\,\mathrm{m^2 s^{-1}}$. These values lead to a mature vortex with a core radius of 3·3 m and a maximum azimuthal velocity, $v_{\max} = 1{\cdot}6\,\mathrm{m\,s^{-1}}$. Although $v_{\max}$ is too small by a factor of four to five for an intense dust devil, it may not be atypical of weak ones, and in any case it corresponds to an angular rotation rate V_e/R, at the 'screen radius', which is only an order of magnitude larger than the Coriolis parameter in mid-latitudes. (A calculation with parameter values typical of a strong dust devil is discussed in section 4.) Again, the value implied for K_M does not seem unreasonable but we are aware of the limitations arising from its use. We regard Expt. 2 of I as the prototype experiment in this paper and refer to it here as Expt. 1.

The most obvious change in the radial boundary conditions must be to allow free flow through the entire boundary. Moreover, the direction of flow must be determined by the dynamics of the flow within the computational region. Accordingly, in all subsequent experiments we take $\partial(ur)/\partial r = 0$ along the whole boundary $r = R$. Through continuity, this implies $w = 0$ at the boundary but it does not seem to impose a severe constraint on the flow, as confirmed by the solutions for different values of R (see section 3). Greater difficulty is encountered in the choice of an appropriate swirling flow condition at $r = R$ as there appear to be a number of possibilities. Mathematically one could prescribe the swirling velocity v, the vertical component of vorticity ζ, or a relation between the two. Ultimately, the choice will depend on what information can be deduced from observations of flow in the vicinity of a dust devil, but as such data have not yet been obtained, we examine two boundary conditions which seem to have most physical relevance and compare these. Thus, for inflowing air ($u < 0$) we specify either $v = V(z)$ or $\zeta = \zeta_e$, a constant, and for outgoing air ($u > 0$) we take $\partial\zeta/\partial r = 0$. The last condition, together with $\partial(ur)/\partial r = 0$, implies zero radial gradient of vorticity flux at $r = R$; i.e. vorticity is advected freely through the side boundary of the computational domain without modification. If the vorticity just inside the boundary is zero, this condition is equivalent to $\partial(vr)/\partial r = 0$ at $r = R$, which implies that outgoing air conserves its angular momentum. However, in a vortical environment, radial changes in circulation are associated with radial gradients in angular momentum and the restriction of angular momentum conservation on air entering or leaving through $r = R$ is too severe.

When ζ is prescribed instead of $V(z)$ at $r = R$, the swirl parameter as defined above is inappropriate and in such cases we choose $Rt = \frac{1}{2}\zeta_e R/V_T$. However, values of this quantity must not be used for comparison of experiments with different values of R, as discussed in section 3.

To complete the boundary conditions at $r = R$ we take $T = T_e$, the ambient temperature, along the entire boundary. An alternative would be to take $T = T_e$ for incoming air and $\partial(rT)/\partial r = 0$ for outgoing air, implying that heat transport away from the region is by

advection only, but it may be shown that these conditions are essentially equivalent as long as the pseudo-Raylcigh number is sufficiently large; see Smith *et al.* (1975).

In the present study we discuss the results of a further series of nine experiments with one of the radial boundary conditions given above, and in some cases with different sizes of computational region to allow the effect of finite domain size on the solutions to be assessed. In these cases we have found it necessary also to permit free slip on part of the lower boundary so that direct comparisons can be made for different values of R, see later. The boundary conditions for these nine experiments are displayed in Fig. 1(b) for comparison with Expt. 1. Specification differences between the experiments are given in Table 1.

TABLE 1. SPECIFICATION DIFFERENCES FOR THE NUMERICAL EXPERIMENTS AND AMPLIFICATION FACTOR A AS CALCULATED FROM THE STEADY VORTEX SOLUTIONS. IN EXPTS. 1 TO 7, $A = (v_{max}/r_{max})/(V_e/R)$; IN EXPTS. 8 TO 10, $A = (v_{max}/r_{max})/\frac{1}{2}\zeta_e$: SEE TEXT

Expt.	R (m)	H (m)	Swirl condition at $r=R$ when $u<0$	Velocity condition at $z=0$	Amplification factor, A
1	40	133	$V = 0{\cdot}23\,\mathrm{m\,s^{-1}}$	no slip	83
2	40	133	$V = 0{\cdot}23\,\mathrm{m\,s^{-1}}$	no slip	86
3	40	133	$V = 0{\cdot}23(1-e^{-0{\cdot}1z})\,\mathrm{m\,s^{-1}}$	no slip	91
4	80	133	$V = 0{\cdot}115\,\mathrm{m\,s^{-1}}$	no slip	72
5	80	133	$V = 0{\cdot}115\,\mathrm{m\,s^{-1}}$	no slip $0<r<40$ m free slip $40<r<80$ m	82
6	40	200	$V = 0{\cdot}23\,\mathrm{m\,s^{-1}}$	no slip	86
7	40	200	$V = \dfrac{0{\cdot}23}{1+(z/25)^4}\,\mathrm{m\,s^{-1}}$	no slip	84
8	40	133	$\zeta_e = 1{\cdot}2\times10^{-2}\,\mathrm{s^{-1}}$	no slip	102
9	80	133	$\zeta_e = 1{\cdot}2\times10^{-2}\,\mathrm{s^{-1}}$	no slip $0<r<40$ m free slip $40<r<80$ m	94
10	120	133	$\zeta_e = 1{\cdot}2\times10^{-2}\,\mathrm{s^{-1}}$	no slip $0<r<40$ m free slip $40<r<120$ m	87

3. DISCUSSION

A description of the basic dynamics of the flows under study is given in I, section 4, and we shall aim here to deduce the differences between these flows and to identify the reasons for these differences. In comparing the flows, a useful measure of vortex strength is the amplification factor A, defined as $(v_{max}/r_{max})/(V_e/R)$, which represents the ratio of angular rotation rate at the radius of maximum azimuthal velocity to that at the lateral boundary of the flow domain. Values obtained for A for the various experiments are given in Table 1.

The isotherms, streamlines, isotachs of swirling velocity and isobars of dynamic pressure for Expts. 1 and 2 are shown in Figs. 2 and 3 respectively. It is evident that the principal differences between these two flows are confined to the neighbourhood of $r = R$. When the flow is allowed to select its own height of inflow, we see that inflow occurs over the whole radial boundary but there is little change in detailed vortex structure and only a very small change in amplification: $A = 86$ compared with 83 in Expt. 1.

In Expt. 3 the azimuthal velocity at $r = R$ falls smoothly from a constant value V_e far above the lower boundary to zero at the boundary itself, instead of remaining constant as in Expt. 2. This sort of profile is more realistic in the atmosphere where the swirling velocity component of the vortex environment about the vortex axis must reduce to zero at the ground. Again, the calculation shows there is little change in flow field structure but the vortex strength is *increased* by about 6%. Thus, although rings of air entering through the

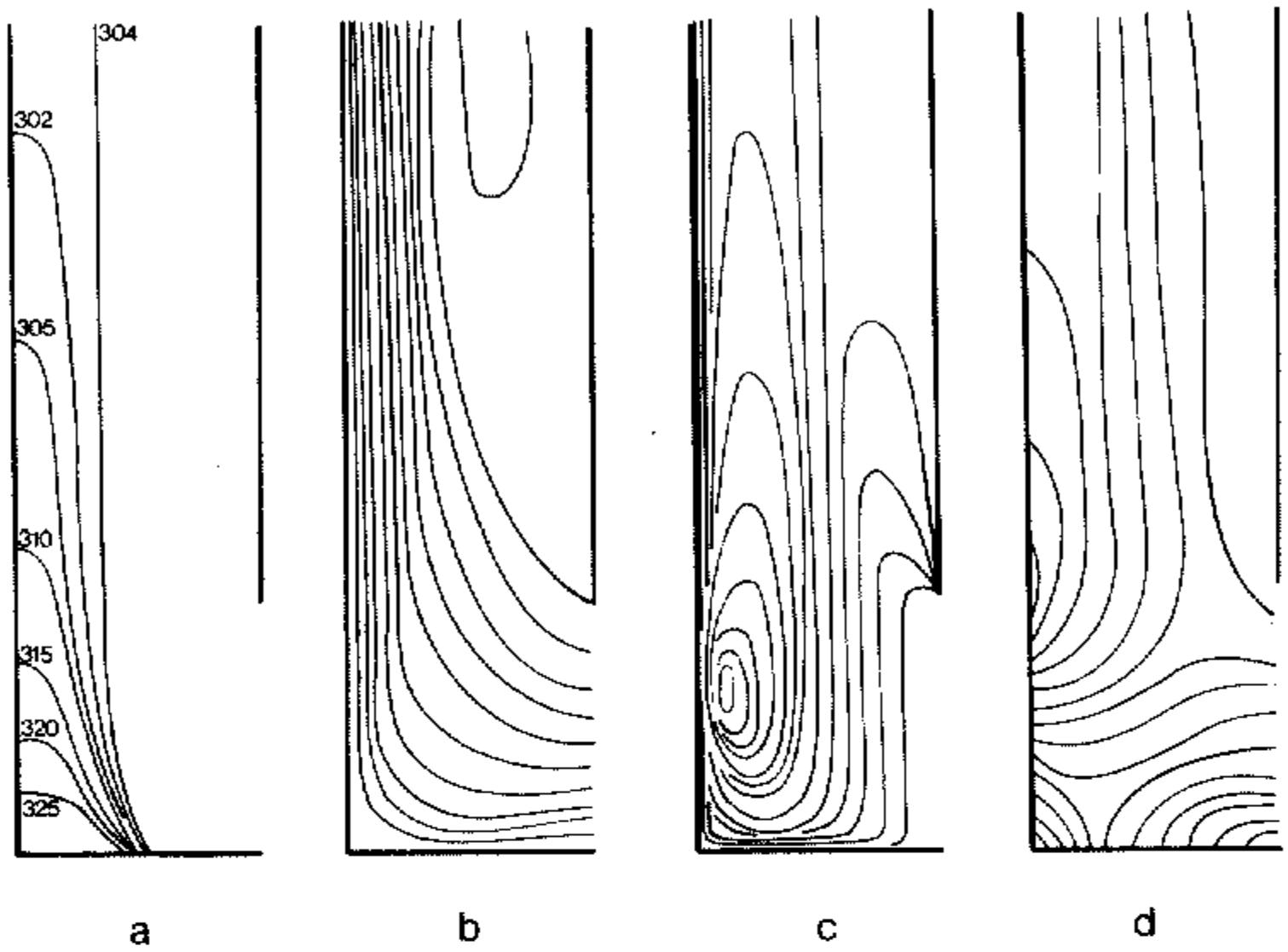

Figure 2. (a) Isotherms (labelled in K); (b) streamlines (contour spacing $4\,m^2s^{-1}$); (c) swirling velocity isotachs (spacing $0{\cdot}2\,m\,s^{-1}$); (d) isobars (spacing 0·2 mb), for Expt. 1.

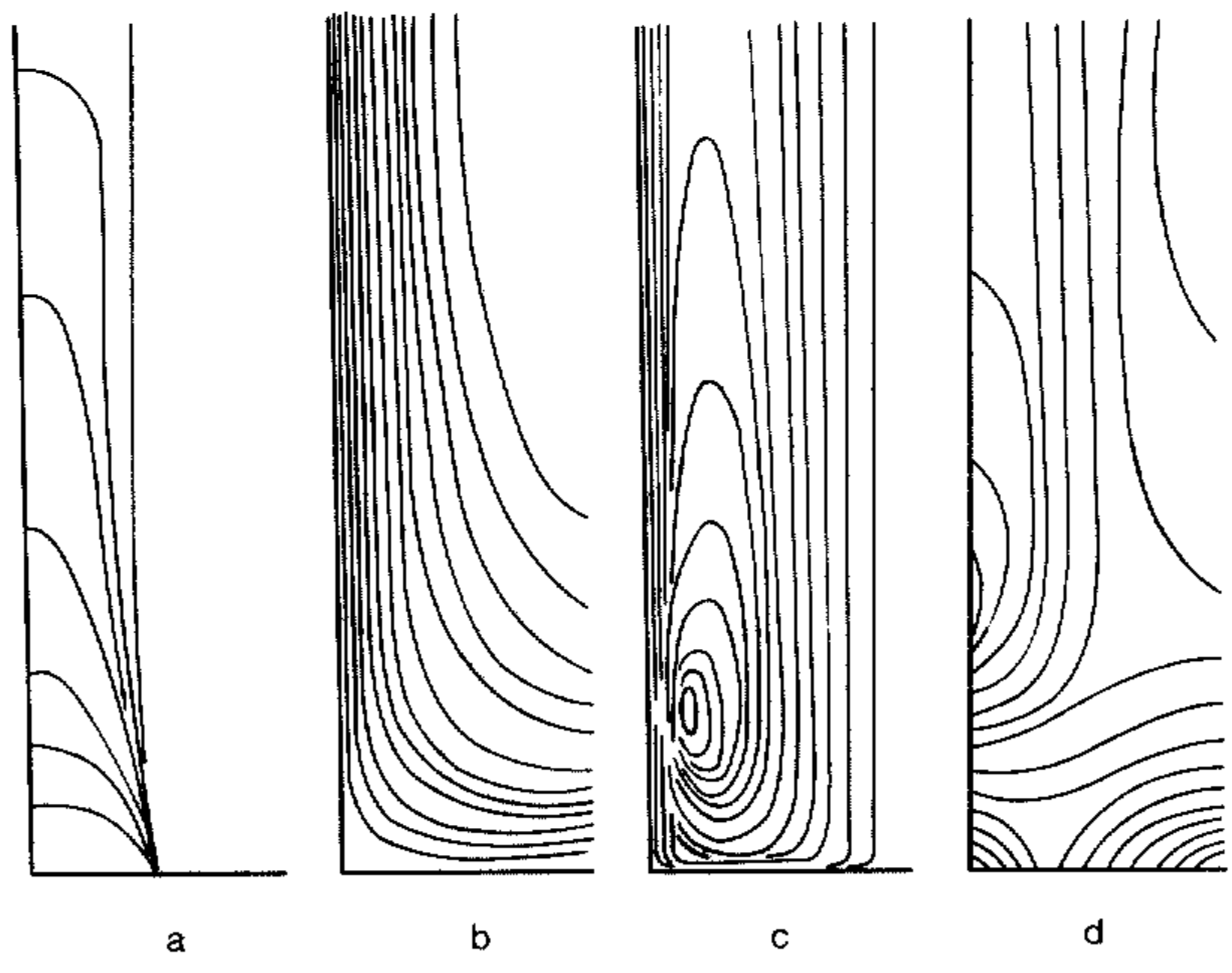

Figure 3. (a) Isotherms; (b) streamlines; (c) swirling velocity isotachs; (d) isobars, for Expt. 2: spacing as in Fig. 2.

side boundary in the lower levels do so with reduced angular momentum, they are able to penetrate a little farther towards the axis before the local centrifugal force and radial pressure gradient achieve balance to prevent subsequent inflow. Accordingly, the increased value for A is associated with a slightly higher swirl velocity maximum attained at a slightly smaller radius.

In seeking to model numerically a laterally unconstrained flow such as a dust devil, we must ensure that the boundary conditions at $r = R$ do not unduly overconstrain the flow in the sense that a different choice of R leads to a radically different flow, qualitatively or

quantitatively or both. So, in Expt. 4 we repeat Expt. 2 with the value of R doubled from 40 to 80 m. With only this change we would not expect to achieve comparability with Expt. 2 since rings of air which enter through the more distant radial boundary have twice the angular momentum of their counterparts. We must therefore double R and halve V_e so that the circulation about the perimeter of the flow at any height, and hence the swirl parameter Rt, remain the same. Even so, the vortex which results is somewhat weaker than in Expt. 2, with $A = 72$ as compared with 86, and this is reflected in the flow fields (not shown) which indicate also a slightly broader vortex core, although there is no qualitative change in flow structure. This result is *not*, however, a reflection of overconstraint at $r = R$ but is largely due to the additional torque exerted on the lower boundary which is quadruple the area of that in Expt. 2. This can be seen by comparing Expt. 2 with Expt. 5, the latter being a rerun of Expt. 4 but with the condition of free slip ($\partial u/\partial z = 0$, $\partial v/\partial z = 0$, $w = 0$) on the lower boundary for $40 < r < 80$ m. The vortices are now closely similar both qualitatively and quantitatively; compare Figs. 4(a) and 4(b) with Figs. 3(b) and 3(c) respectively; and in Expt. 5 the amplification factor is 82 which is close to that in Expt. 2. Furthermore, the closeness of the streamline patterns near $r = 40$ m in the two calculations suggests that the condition $w = 0$ at the lateral boundary of the computational domain does not unduly overconstrain the flow.

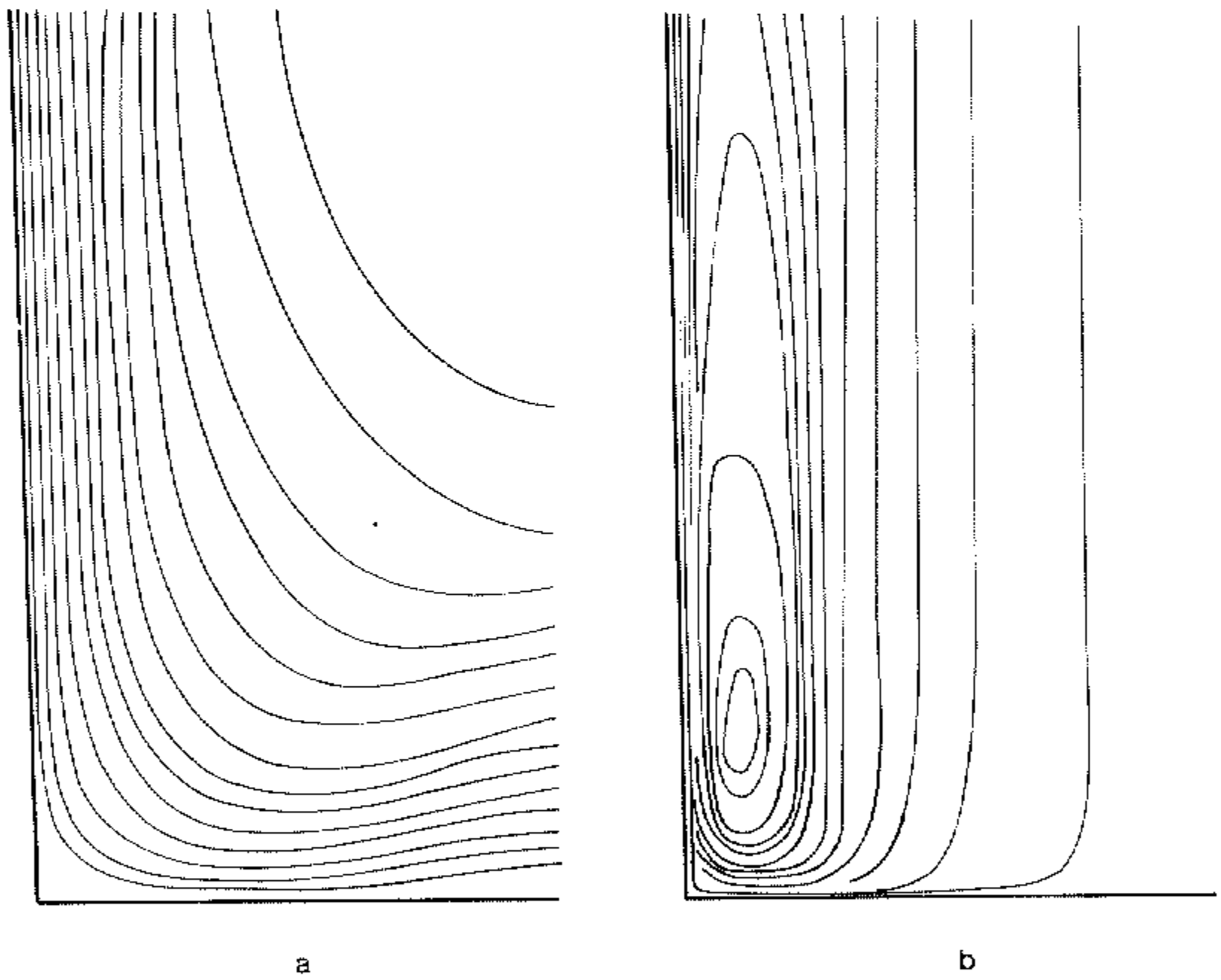

Figure 4. (a) Streamlines; (b) swirling velocity isotachs, for Expt. 5: spacing as in Fig. 2.

We wish to emphasize that the calculation with free slip on part of the lower boundary is not conceived as a further step towards physical realism, which it clearly is not, but is carried out to enable the effect of the additional torque to be estimated. However, it is opportune to point out that in any atmospheric vortex model, the size of the computational region will inevitably be a parameter in the calculation of vortex strength as it determines the area of the lower boundary available for exerting torque.

Experiment 6 is a repeat of Expt. 2 with the height of the computational region extended by a factor of 1·5 and provides a means of assessing the upper boundary conditions. As can be seen by comparing Figs. 5(a), (b) with Figs. 3(b), (c), respectively, the velocity fields

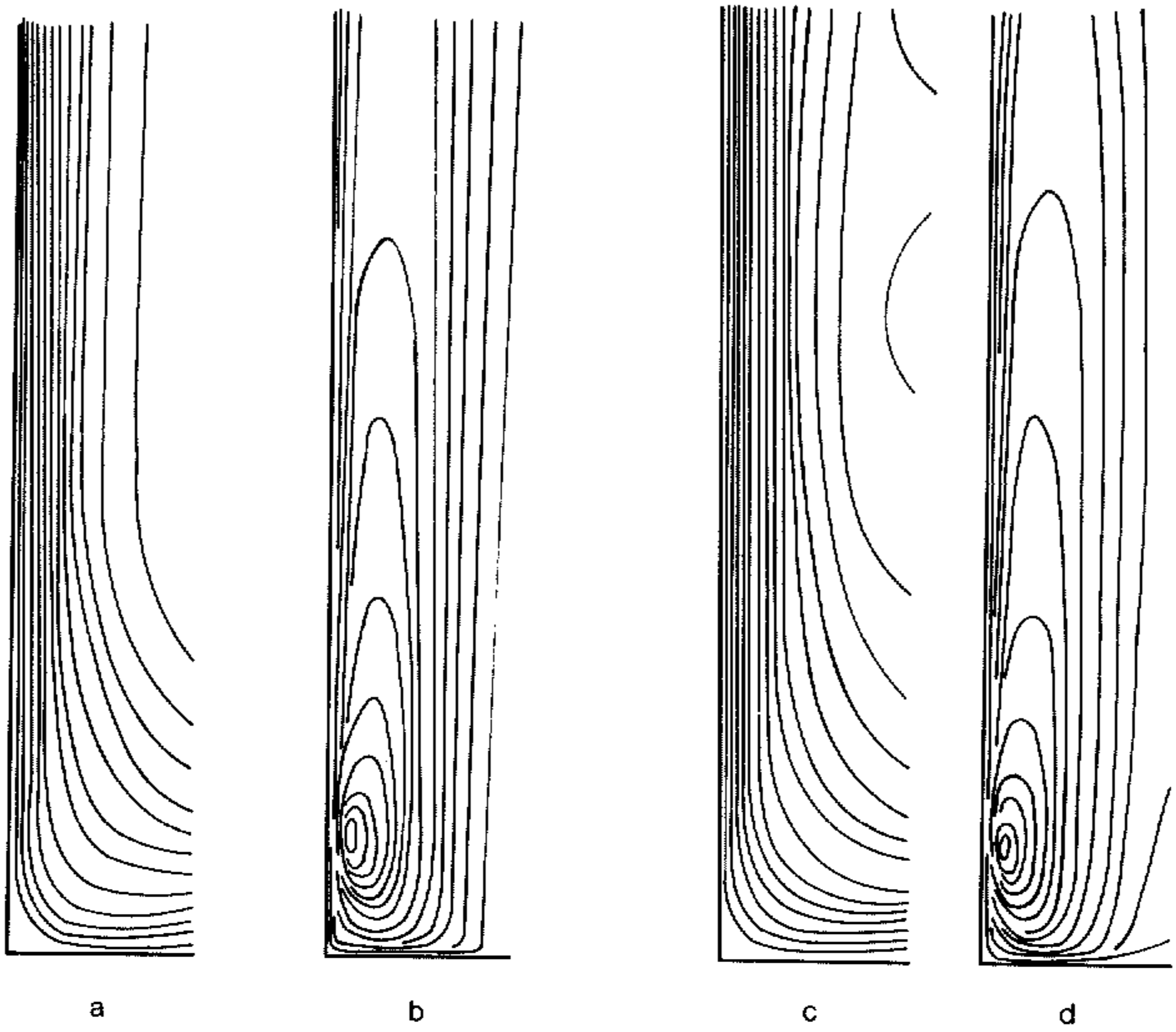

Figure 5. (a) Streamlines; (b) swirling velocity isotachs, for Expt. 6; (c) streamlines; (d) swirling velocity isotachs for Expt. 7: spacing as in Fig. 2.

in the two experiments are almost identical in their region of overlap; moreover, the amplification factor, which is quite sensitive to small changes in the swirling velocity field, is the same in each case. We may therefore conclude that the upper boundary conditions create little unintended constraint on free flow through that boundary.

It is now interesting to compare Expts. 6 and 7 which are identical except that in the latter the swirling velocity at $r = R$ is taken to be $V(z) = V_e/\{1+(z/25)^4\}$ for incoming air, rather than simply a constant V_e as in the former case (z in metres). Thus, in Expt. 7 we explore the effect on vortex dynamics of having a field of rotation which is concentrated primarily at low levels. In this situation, the streamlines show a region of outflow through the side boundary at intermediate heights, sandwiched between regions of inflow, see Fig. 5(c). This feature may be given a physical interpretation as follows. Since the imposed circulation at $r = R$ decreases sharply with height, rings of air which enter at lower levels and are advected upwards find themselves in an environment where the circulation decreases with increasing radius. It appears that at intermediate heights and near the perimeter of the computational domain, the resulting excess centrifugal force on the ring is sufficient to overcome the local, inward, radial pressure gradient causing an outward drift of air. However, at larger heights, the rotational constraints are reduced and the outward drift is reversed owing to the continued buoyant acceleration of the flow and the entrainment it produces.

At present there are few detailed observational data on the wind fields of a dust devil environment; in particular, the vertical extent of the background rotation is not known. However, our calculations suggest that if the rotation source is concentrated at low levels, there may be evidence of outflow, or of centrifugal instability, at intermediate heights.

We now go on to consider the choice of swirling flow condition at $r = R$, and its implications. In all the previous experiments, the swirling velocity is specified at this radius and since inflowing air approximately conserves its angular momentum as it enters through the side boundary, the radial gradient of circulation is very nearly zero and there is negligible inward advection of vertically oriented vorticity. Thus, vertically oriented vortex lines along the vortex core must emanate from the ground boundary layer region where they are roughly horizontal. Moreover, in the outer part of the vortex, the swirling flow is approximately irrotational with azimuthal velocity decaying as $1/r$. Whilst Sinclair's observations show that the swirling velocity field in a dust devil does approximate this type of behaviour (Sinclair 1973, p. 1609), it is unlikely that the dust devil environment is entirely devoid of vertically orientated vorticity and it is of considerable interest to compare Expt. 2 with Expt. 8, in which the vertical vorticity ζ_e is prescribed for inflowing air at $r = R$, instead of the swirling velocity. To permit quantitative comparison between these experiments, we take $\zeta_e = 2V_e/R$.

The streamlines and isotachs of swirling velocity for Expt. 8 are shown in Figs. 6(a) and 7(a) respectively. It is clear that no new flow features are present when ζ_e is prescribed although the vortex is stronger, with amplification factor, defined in this case by $(v_{max}/r_{max})/\frac{1}{2}\zeta_e$, equal to 102 as compared with 86 in Expt. 2. Nevertheless, the vorticity fields differ as can be seen by comparing Figs. 8(a) and 8(b), which show contours of equal circulation, rv, for Expts. 2 and 8 respectively. In Expt. 2 the circulation decreases with decreasing radius in all parts of the flow although circulation gradients outside the vortex core are relatively small. This is consistent with there being a sink of angular momentum at the lower boundary. In Expt. 8, however, there is an extensive region of flow where the circulation increases with decreasing radius adjacent to the core. This increase is due to the vertical stretching of ambient vorticity as converging air accelerates upwards but it should be emphasized that radial circulation gradients are not especially large and the swirling velocity outside the core does not depart significantly from a $1/r$ profile.

Without further guidance from observations, it is difficult to argue a preference for

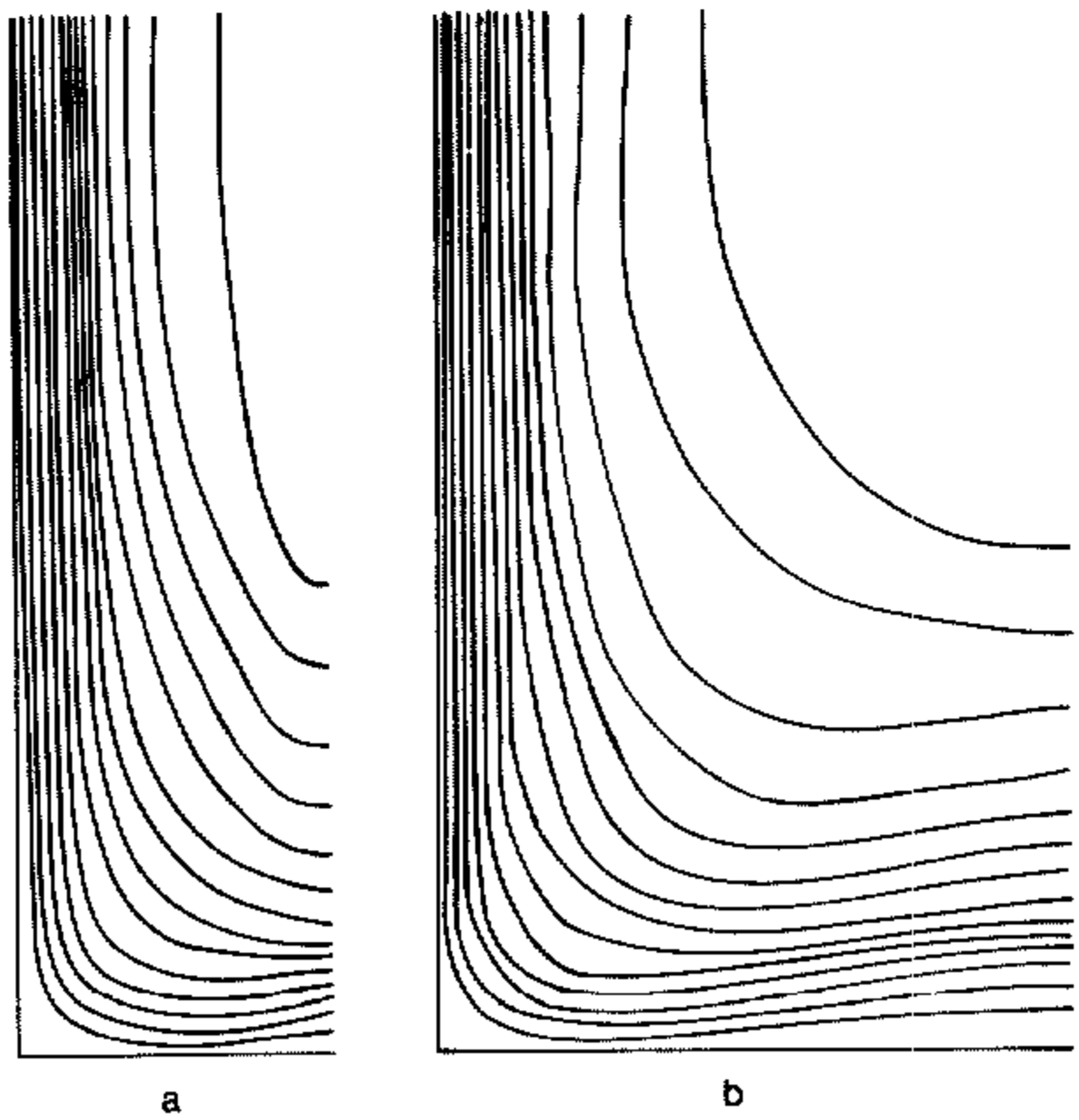

Figure 6. Streamlines for: (a) Expt. 8; (b) Expt. 9: spacing $4\,m^2s^{-1}$.

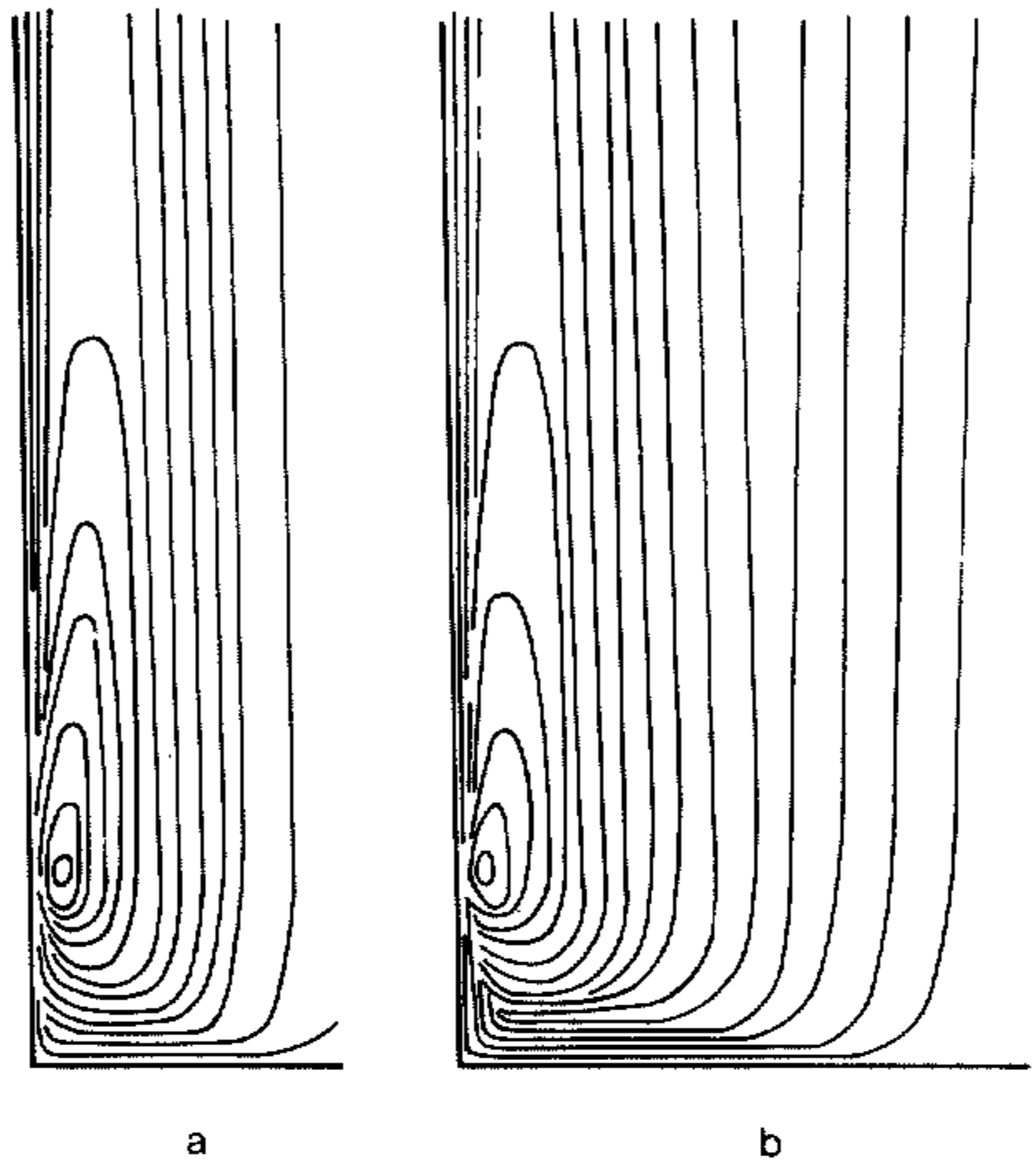

Figure 7. Swirling velocity isotachs for: (a) Expt. 8; (b) Expt. 9: spacing 0·2 m s^{-1}.

either of the two swirling conditions studied. Even so, it is important to know what implications a particular choice will have on the ensuing dynamics and to be aware of any changes which might arise if the radius of the computational domain is extended. We have already studied the latter question in relation to Expt. 2 and have seen that if R is increased and the circulation imposed at R remains fixed, the vortices obtained are comparable in structure but the extra torque at the lower boundary reduces the vortex strength. However, in the case of Expt. 8, it is not immediately clear how ζ_e should be changed as R is changed to achieve the same rotational constraint. If $(\partial\zeta/\partial r)_{r=R}$ is zero, or sufficiently small, at heights where ζ_e is prescribed, the boundary condition $\zeta(R, z) = \zeta_e$ is equivalent, or approximately equivalent, to the specification of solid-body rotation with angular velocity $\frac{1}{2}\zeta_e$ at that radius. Hence if we change R, we must presumably keep ζ_e constant. We would not then expect the flow outside the core to be similar for all values of R, even with the boundary conditions we have chosen at this radius, since with solid-body rotation at large radial distances and a given strength of forcing, there is always some radial length scale R_L beyond which the flow will be largely unaffected by the presence of the vortex. This is well demonstrated in the laboratory experiments of Turner (1966) where vortices are generated in a rotating tank of water with vertical axis by releasing a steady stream of air bubbles along the axis of rotation. The rising bubbles cause a meridional circulation in the water, strong enough to produce a concentrated vortex along the rotation axis but too weak to influence fluid near the sides of the container. In this situation, the circulation is terminated by a free shear layer and hence R_L is smaller than the container radius.

If in our experiments $R < R_L$, we might expect broad similarity between flows for different values of R and we have therefore repeated Expt. 8 with R increased twofold (Expt. 9) and threefold (Expt. 10) to explore this possibility. To permit quantitative comparison of these last two experiments with Expt. 8 we have again taken the condition of free slip on the lower boundary for $r > 40$ m as in Expt. 5.

Firstly, we note that the calculations for Expts. 8, 9 and 10 show that $\zeta_e^{-1}(\partial\zeta/\partial r)_{r=R}$ is small (maximum value about $0{\cdot}03\,\mathrm{m}^{-1}$) at heights where ζ_e is prescribed so that the boundary condition $\zeta(R,z) = \zeta_e$ is closely equivalent to the specification of solid-body rotation with angular velocity $\frac{1}{2}\zeta_e$ at the radius. It may help to understand this result if we consider the quation for axial vorticity which together with the boundary conditions at $r = R$ gives

$$\left[u\frac{\partial}{\partial r} - \frac{K_M}{r}\frac{\partial}{\partial r}r\frac{\partial}{\partial r}\right]\zeta = -\frac{\partial v}{\partial z}\frac{\partial w}{\partial r} \qquad \text{at } r = R,$$

when $\zeta_e(R,z)$ is prescribed. Hence, ignoring diffusion which is relatively small in our experiments, radial gradients of axial vorticity near $r = R$ are produced by the tilting of radial vorticity by radial gradients of vertical velocity. It is evident from Figs. 6 and 7 that the largest values of $\partial v/\partial z$ occur near the lower boundary, where the streamlines are more horizontal and hence values of $\partial w/\partial r$ are small, whereas values of $\partial v/\partial z$ are small at larger heights where $\partial w/\partial r$ is appreciable; for this reason, the term $(\partial v/\partial z)(\partial w/\partial r)_{r=R}$ in the above equation remains uniformly small.

The streamlines and isotachs of swirling velocity for Expt. 9 are shown in Figs. 6(b) and 7(b) respectively. It is clear that the vortices in Expts. 8 and 9 are comparable in structure

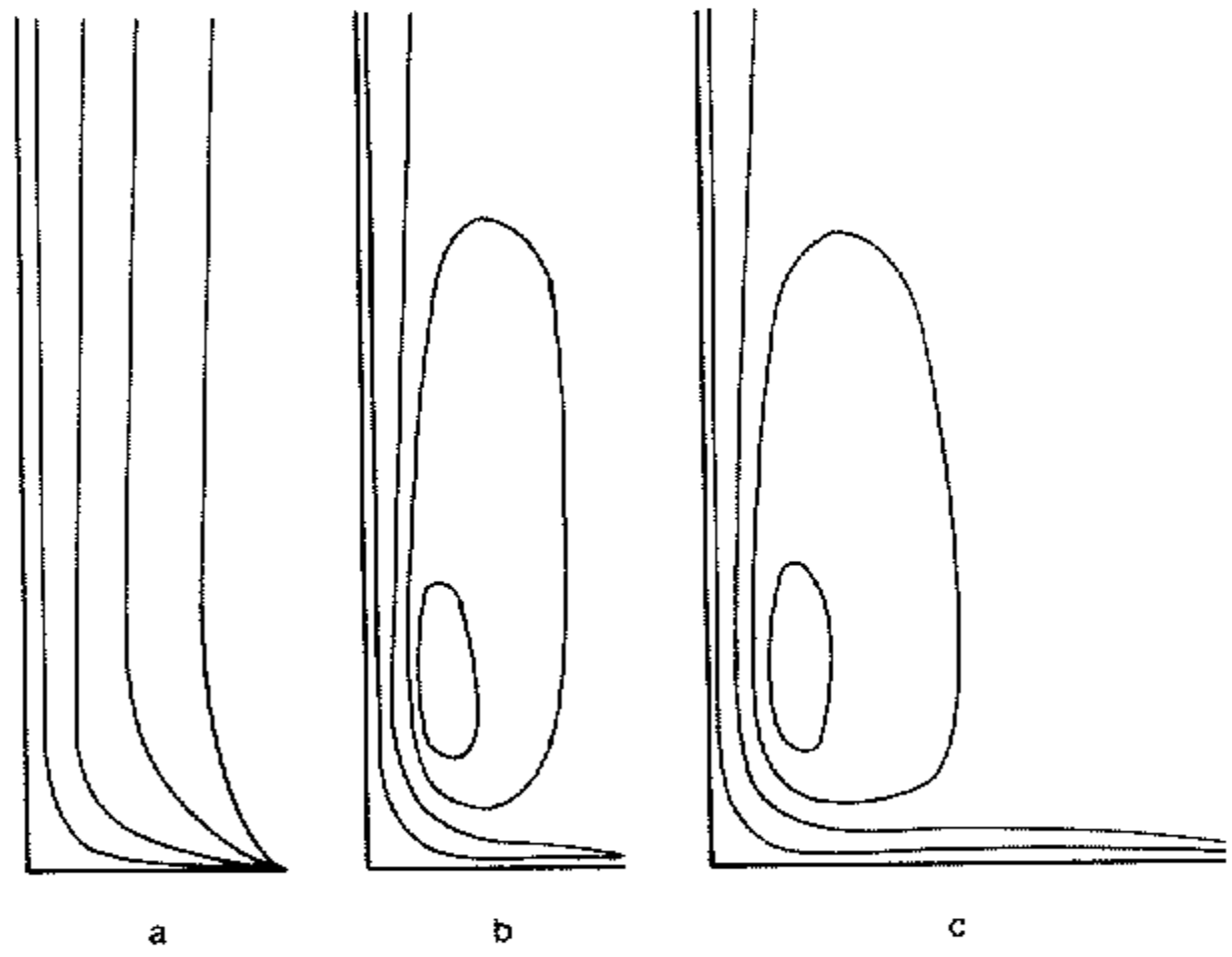

Figure 8. Isopleths of circulation rv for: (a) Expt. 2; (b) Expt. 8; (c) Expt. 9: spacing $0{\cdot}4\,\mathrm{m^2 s^{-1}}$.

and the patterns of circulation are broadly similar (cf. Figs. 8(b) and 8(c)); this is also true for Expt. 10 (velocity fields not shown). However, even when the extra ground torque has been compensated for by taking the condition of free slip on $z = 0$ for $r > 40\,\mathrm{m}$, the amplification factor decreases to some degree as R increases: i.e. $A = 102$, 94 and 87 in Expts. 8, 9 and 10, respectively.

4. Strong dust devil solutions

As discussed in section 2, our choice of nondimensional parameters (principally Ra and Rt) was made to allow comparison of the present experiments with those in I, but it was seen that, with suitable geometrical scales, these parameters lead to a rather weak dust devil vortex. Recently our computer facilities have improved, enabling us to explore parameter values a little further and we have now also found values which correspond with dust devils of moderate strength.

If we take $T_e = 300\,\mathrm{K}$, $R = 40\,\mathrm{m}$, $H = 133\,\mathrm{m}$ as before and take $T_s = 330\,\mathrm{K}$ with

$R_s = 40\,\mathrm{m}$ (i.e. heating over the entire lower boundary), $K_M = 0{\cdot}2\,\mathrm{m^2 s^{-1}}$ and $\zeta_e = 8 \times 10^{-2}\mathrm{s^{-1}}$, we obtain a two-celled vortex with downflow on the whole axis; a maximum swirling velocity of $7{\cdot}9\,\mathrm{m\,s^{-1}}$ occurring at 6·1 m radius; a maximum vertical velocity $w_{\max} = 9{\cdot}1\,\mathrm{m\,s^{-1}}$, a maximum downflow velocity $w_{\min} = 2{\cdot}9\,\mathrm{m\,s^{-1}}$, an amplification factor of 30 and a pressure drop Δp across the core at ground level equal to 2·1 mb. Except for the values of K_M, data for which have not been obtained, these values are comparable with the detailed measurements for dust devil No. 1 made by Sinclair although the vortex here is a little weaker and marginally broader and has circulation $v_{\max} r_{\max} = 48\,\mathrm{m^2 s^{-1}}$, compared with about $61\,\mathrm{m^2 s^{-1}}$ for dust devil No. 1.

A reduction in ζ_e to $5 \times 10^{-2}\mathrm{s^{-1}}$ decreases the vortex strength and the radius at which the maximum swirl is attained; now $v_{\max} = 6{\cdot}0\,\mathrm{m\,s^{-1}}$ and $r_{\max} = 5{\cdot}1$ m, whereas the amplification factor is increased to 42. Also, $w_{\max}$ reduces to $7{\cdot}1\,\mathrm{m\,s^{-1}}$, $w_{\min}$ decreases to $2{\cdot}5\,\mathrm{m\,s^{-1}}$ but the pressure drop, now 2·0 mb, is barely changed. These effects are anticipated from the discussion given in I, section 4.

Finally, since observations provide little guidance in the choice of K_M, we have repeated the above calculations with $K_M = 0{\cdot}4\,\mathrm{m^2 s^{-1}}$ to assess their sensitivity to the selected diffusivity. In each case $v_{\max}$, $r_{\max}$, Δp and even A are virtually unchanged, suggesting that the dynamical factors which regulate these aspects of the flow are essentially inviscid. However, again as anticipated, an increase in K_M increases the axial decay and radial spread of the swirling velocity field which implies (see I, Eq. (5)) a larger adverse, axial pressure gradient. Hence $w_{\max}$ is reduced and $w_{\min}$ increased; when $\zeta_e = 8 \times 10^{-2}\mathrm{s^{-1}}$, $w_{\max} = 8{\cdot}7\,\mathrm{m\,s^{-1}}$ and $w_{\min} = 3{\cdot}2\,\mathrm{m\,s^{-1}}$; when $\zeta_e = 5 \times 10^{-2}\mathrm{s^{-1}}$, $w_{\max} = 6{\cdot}9\,\mathrm{m\,s^{-1}}$ and $w_{\min} = 2{\cdot}8\,\mathrm{m\,s^{-1}}$.

5. Conclusion

In this paper and its predecessor, we are able to account for the principal dynamical features of dust devils (excluding vortex breakdown) in terms of a numerical model of a thermally driven vortex. In I, the calculations are performed for a laboratory flow configuration, but it is argued that the model contains the two main ingredients of a dust devil (i.e. strong thermal forcing from below in the presence of rotation) and therefore that the strong dynamical coupling between the axial and azimuthal flow fields in the model, which the calculations help to elucidate, are essentially the same in dust devils.

Here, we have sought to model a dust devil more closely, concentrating mainly on a more realistic representation of its environment by the choice of an appropriate radial boundary condition. As part of this we take the vertical velocity to be zero: this is only a weak constraint on the meridional circulation provided that the boundary is sufficiently far from the axis, and it also allows the flow itself to determine the height over which inflow occurs. The condition is completed by prescribing the ambient air temperature and a condition on the swirling velocity field. As regards the latter, the mathematical problem is well-posed when the swirling velocity, or the axial component of vorticity or a relationship between the two, is prescribed. However, it is not possible to select the most physically realistic of these conditions on the basis of currently available data and we have therefore compared calculations in which either the swirling velocity or the axial vorticity component is specified at levels where inflow occurs. At the other levels the radial gradient of axial vorticity is taken to be zero. It is shown that apart from a modest difference in vortex strength, and from small differences in the pattern of circulation outside the vortex core, the two flows are closely similar. In particular, the dynamical constraints on the vortex core are insensitive to the exact nature of the ambient source of rotation, a fact which confirms the applicability to dust devils of the discussion given in I.

Finally, we have obtained vortex solutions which are comparable both qualitatively and quantitatively with observed data for a moderately intense dust devil and have shown that these solutions are not especially sensitive to the value taken for the eddy diffusivities.

Much of the foregoing discussion is relevant to other types of sub-synoptic-scale vortices including tornadoes and waterspouts and should prove helpful in the formulation of models for these. It should also serve as useful guidance in the design of future observational studies of dust devils and their immediate environment.

Acknowledgment

We have benefited greatly from the many stimulating discussions about vortices which we have had over the years with Bruce Morton.

References

Barcilon, A. 1967 A theoretical and experimental model for a dust devil, *J. Atmos. Sci.*, **24**, 453–466.

Fitzgarrald, D. E. 1973 A laboratory simulation of convective vortices, *Ibid.*, **30**, 894–902.

Sinclair, P. C. 1973 The lower structure of dust devils, *Ibid.*, **30**, 1599–1619.

Smith, R. K., Morton, B. R. and Leslie, L. M. 1975 The role of dynamic pressure in generating fire wind, *J. Fluid Mech.*, **68**, 1–19.

Smith, R. K. and Leslie, L. M. I 1976 Thermally driven vortices: a numerical study with application to dust devil dynamics, *Quart. J. R. Met. Soc.*, **102**, 791–804.

Turner, J. S. 1966 The constraints imposed on tornado-like vortices by the top and bottom boundary conditions, *J. Fluid Mech.*, **25**, 377–400.